

Supporting Information

Hierarchical design of $\text{Cu}_{1-x}\text{Ni}_x\text{S}$ nanosheets for high-performance asymmetric solid-state supercapacitors

Jayaraman Balamurugan,^a Chao Li,^a Tran Duy Thanh,^a Ok-Kyung Park,^{a*} Nam Hoon Kim^a
and Joong Hee Lee^{a,b*}

^aAdvanced Materials Institute of BIN Convergence Technology (BK21 Plus Global) & Dept.
of BIN Convergence Technology, Chonbuk National University, Jeonju, Jeonbuk 561-756,
Republic of Korea.

^bCarbon Composite Research Centre, Department of Polymer –Nano Science and
Technology, Chonbuk National University, Jeonju, Jeonbuk 561-756, Republic of Korea

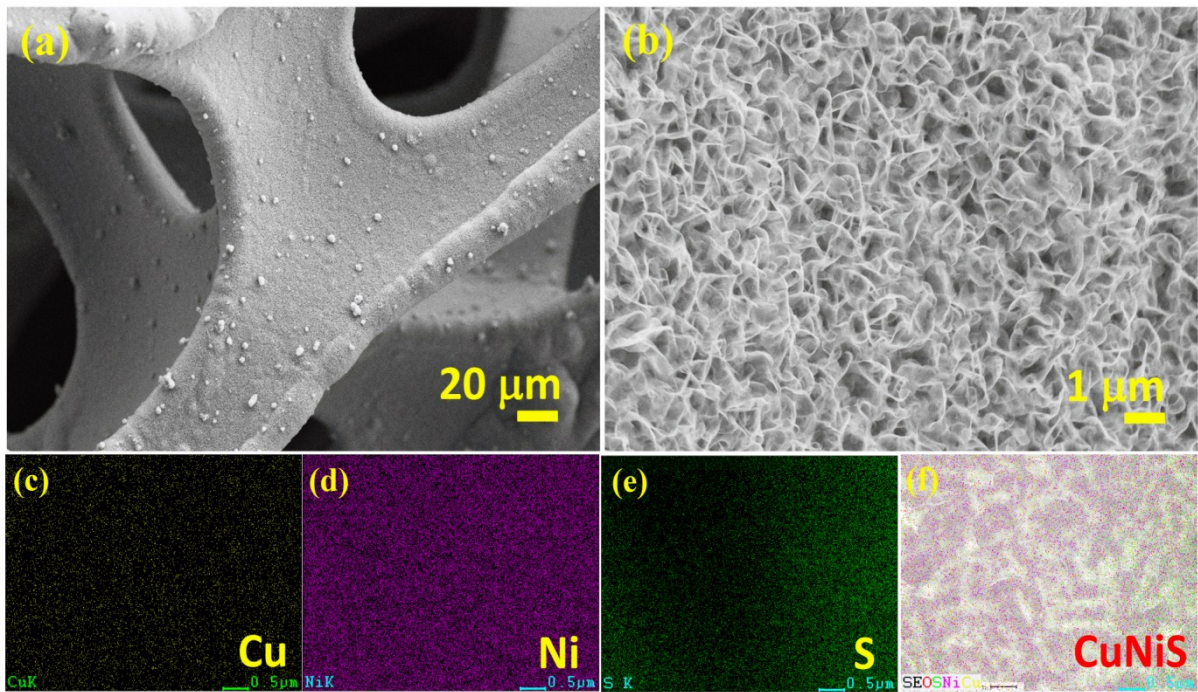


Fig. S1. (a, b) SEM images with different magnification of $\text{Cu}_{1-x}\text{Ni}_x\text{S}$ nanosheet arrays, (c–f) SEM-EDS color mappings of copper, nickel and sulfur in the $\text{Cu}_{1-x}\text{Ni}_x\text{S}$ nanosheet arrays.

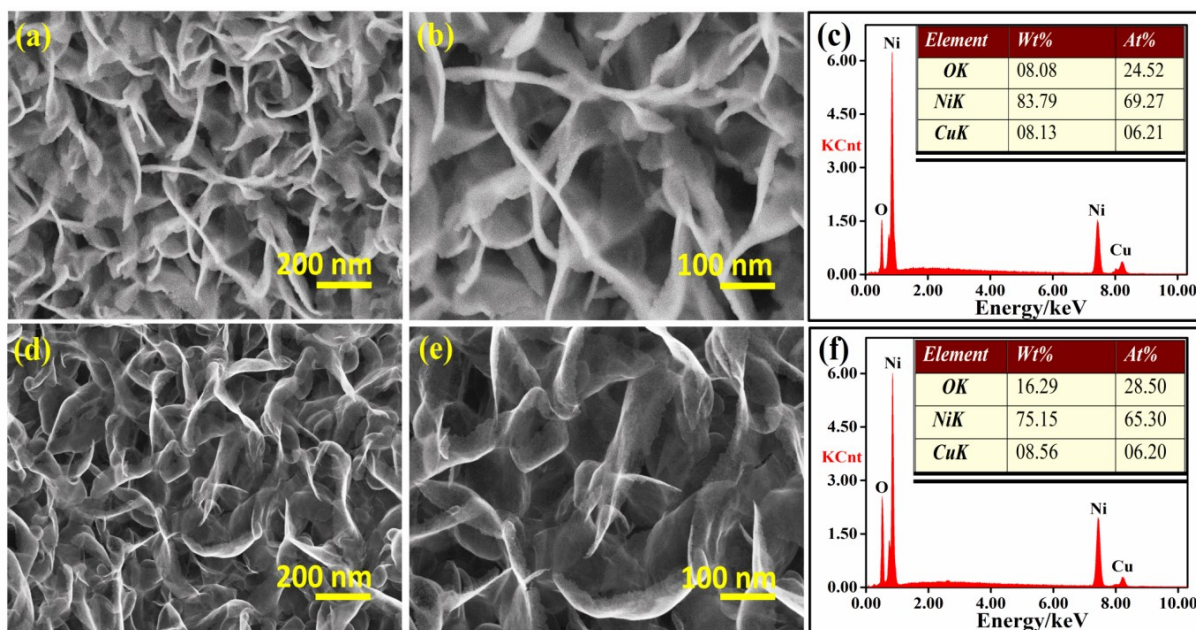


Fig. S2. (a, b) SEM images with different magnification, (c) EDAX spectrum of Cu_{1-x}Ni_x DHs supported on porous 3D Ni backbone, (d, e) SEM images with different magnifications, (f) EDAX spectrum of Cu_{1-x}Ni_xO nanosheet arrays on porous 3D Ni backbone.

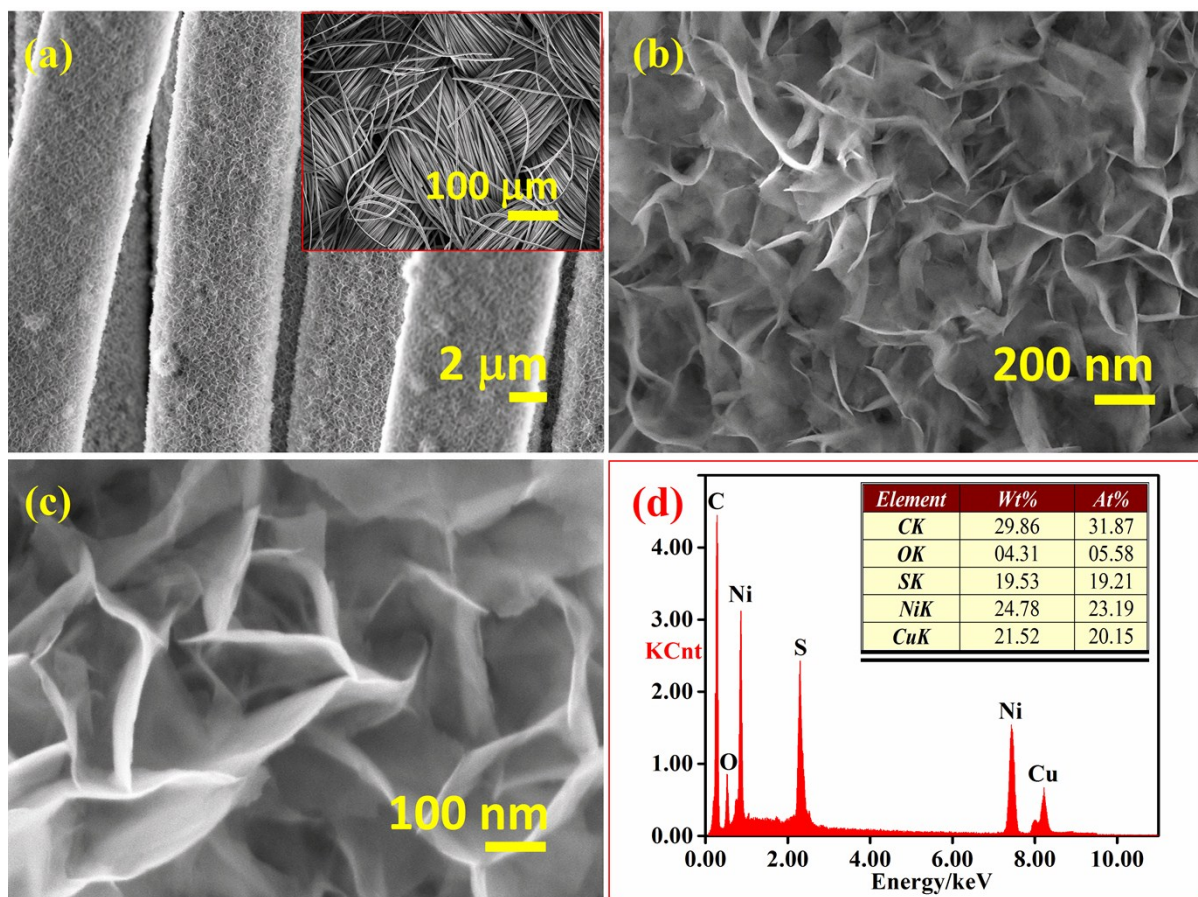


Fig. S3. (a-c) SEM images with different magnification, and (d) EDAX spectrum of $\text{Cu}_{1-x}\text{Ni}_x\text{S}$ nanosheet arrays supported on carbon cloth.

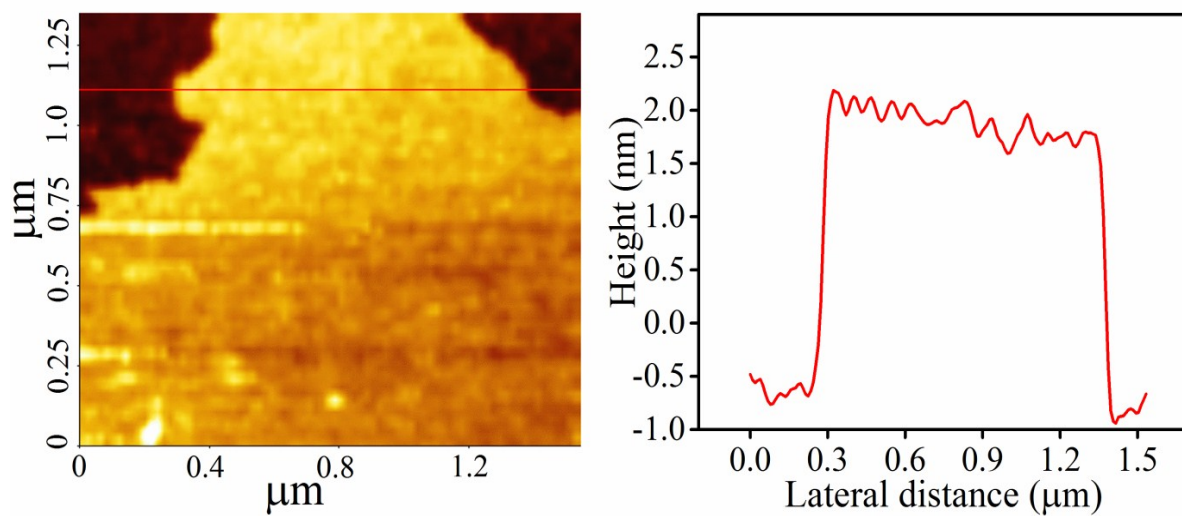


Fig. S4. 2D AFM image and its height profile of Cu_{1-x}Ni_xS nanosheet arrays representing thickness of few nm and width > 2 μm.

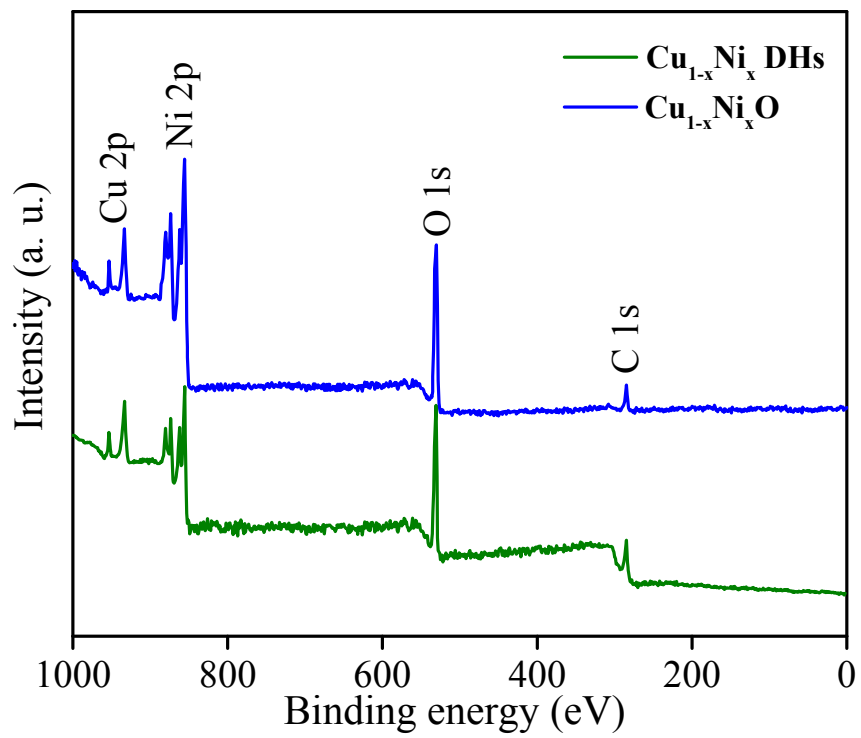


Fig. S5. XPS survey spectrum of $\text{Cu}_{1-x}\text{Ni}_x$ DHs and $\text{Cu}_{1-x}\text{Ni}_x\text{O}$ nanosheet arrays.

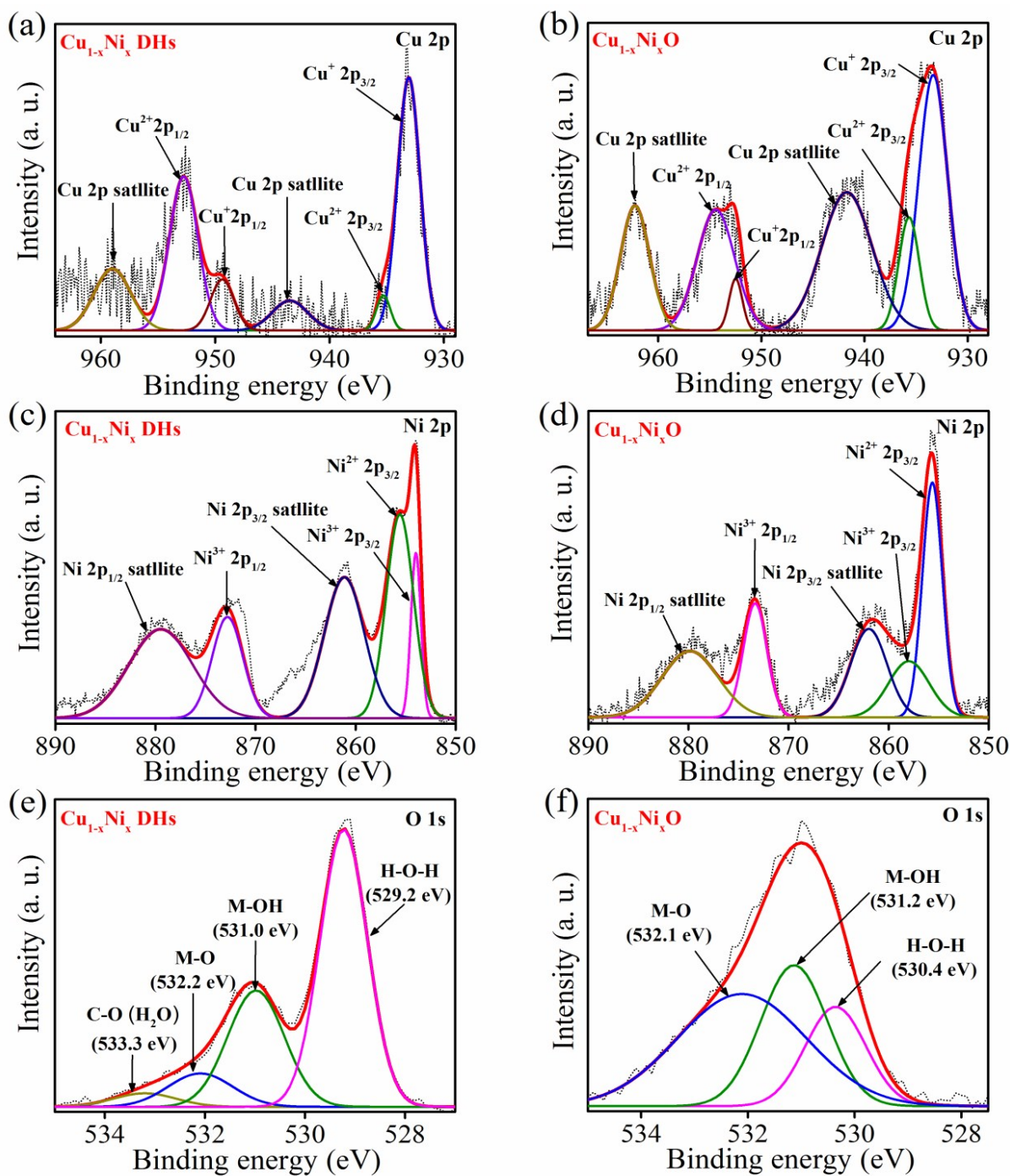


Fig. S6. (a, b) Cu 2p spectra, (c, d) Ni 2p spectra, and (e, f) O 1s spectra of $\text{Cu}_{1-x}\text{Ni}_x$ DHs and $\text{Cu}_{1-x}\text{Ni}_x\text{O}$ nanosheet arrays, respectively.

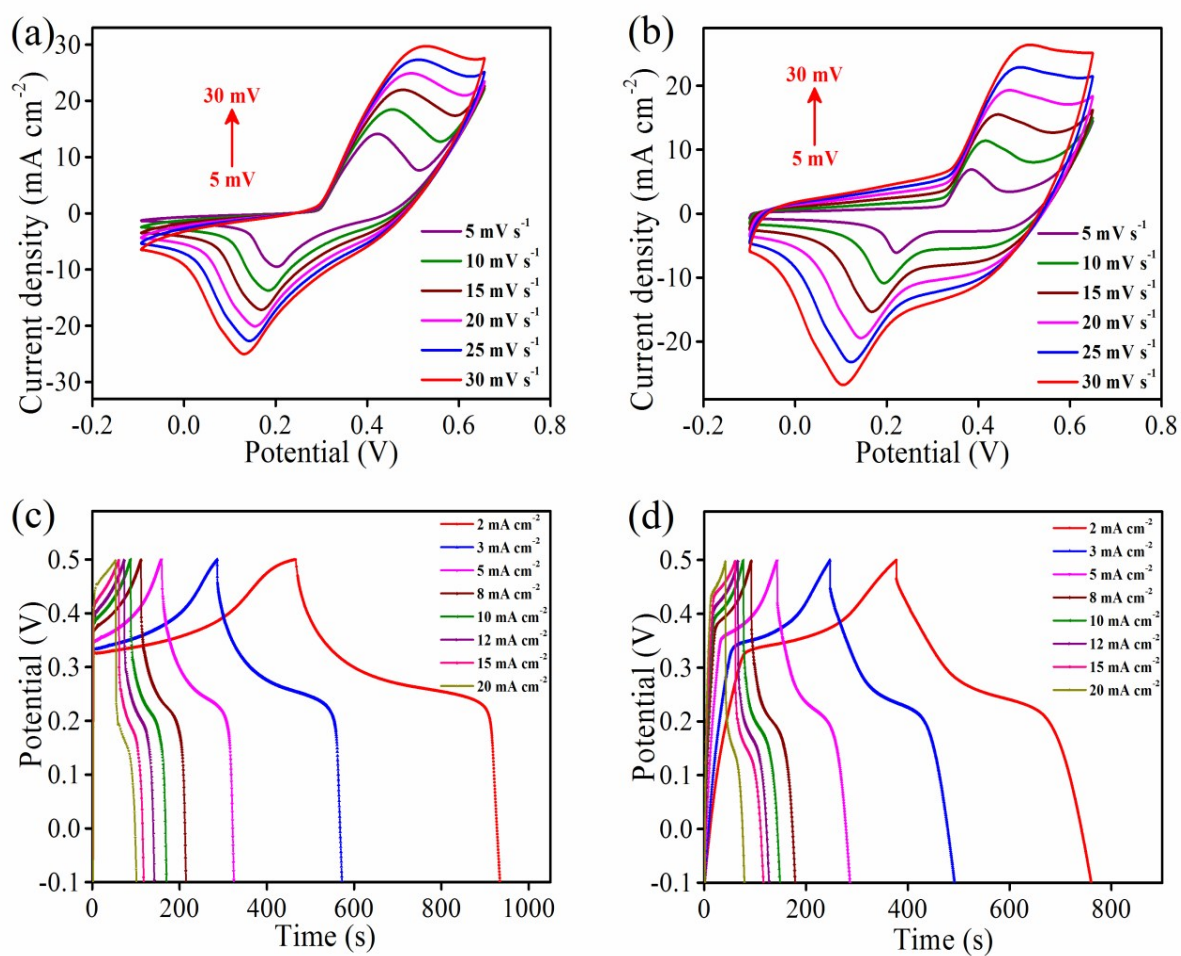


Fig. S7. CV curves with different sweep rates of (a) $\text{Cu}_{1-x}\text{Ni}_x$ DHs, (b) $\text{Cu}_{1-x}\text{Ni}_x\text{O}$ electrodes; GCD curves at different current density of (c) $\text{Cu}_{1-x}\text{Ni}_x$ DHs, and (d) $\text{Cu}_{1-x}\text{Ni}_x\text{O}$ electrodes.

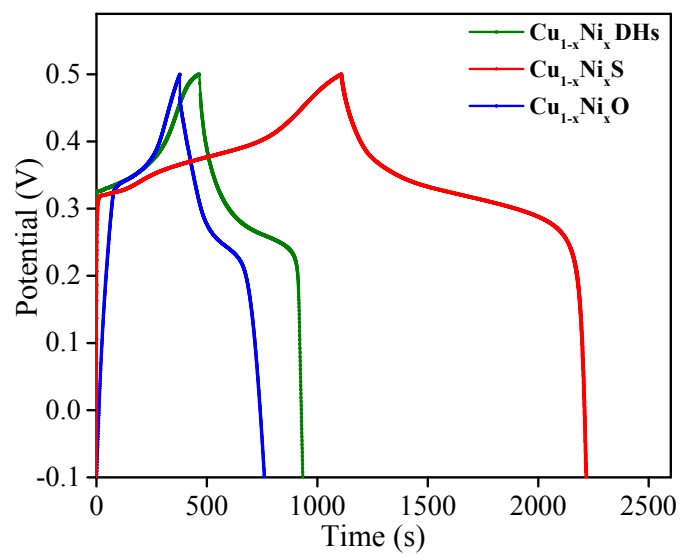


Fig. S8. GCD curves of $\text{Cu}_{1-x}\text{Ni}_x$ DHs, $\text{Cu}_{1-x}\text{Ni}_x\text{O}$, and $\text{Cu}_{1-x}\text{Ni}_x\text{S}$ electrodes at a current density of 2 mA cm^{-2} .

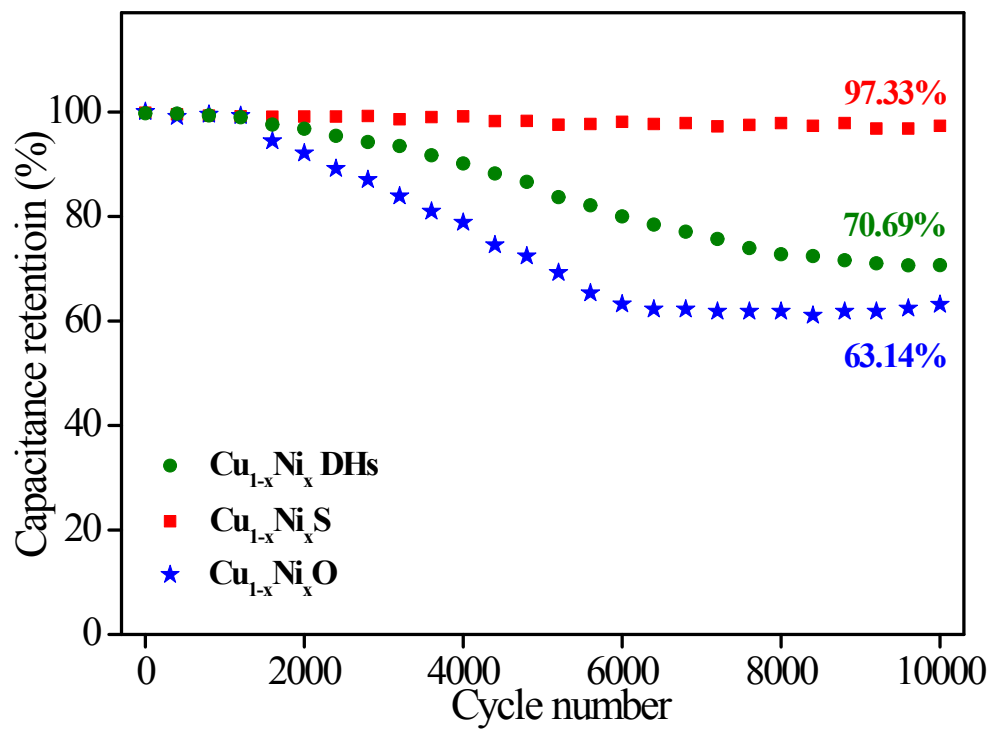


Fig. S9. Cycling performance of $\text{Cu}_{1-x}\text{Ni}_x$ DHs, $\text{Cu}_{1-x}\text{Ni}_x\text{O}$, and $\text{Cu}_{1-x}\text{Ni}_x\text{S}$ electrodes at a current density of 12 mA cm^{-2} .

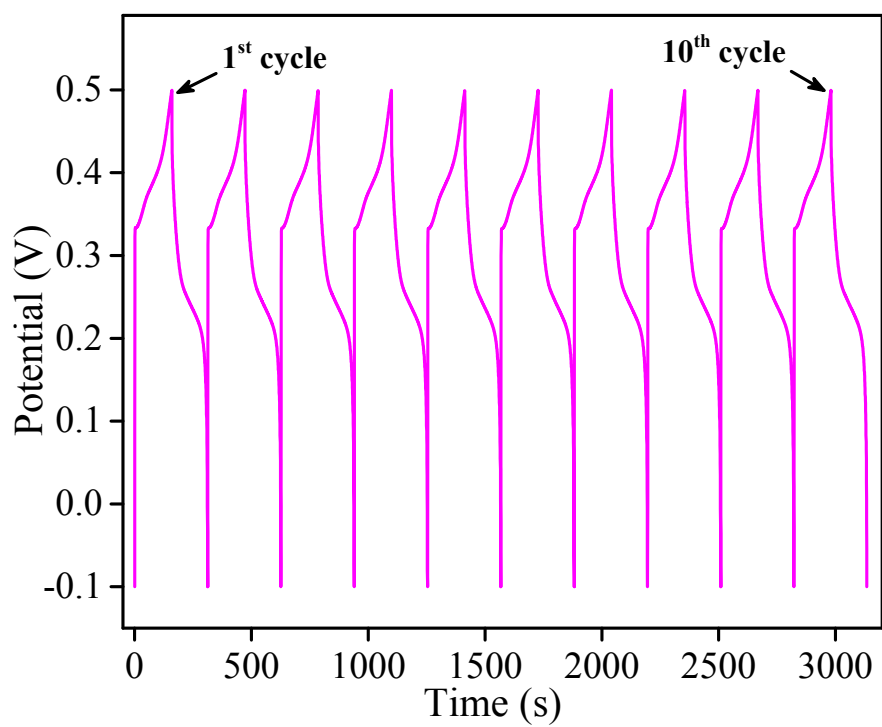


Fig. S10. GCD curves of $\text{Cu}_{1-x}\text{Ni}_x\text{S}$ electrode: from the 1st to 10th cycles test.

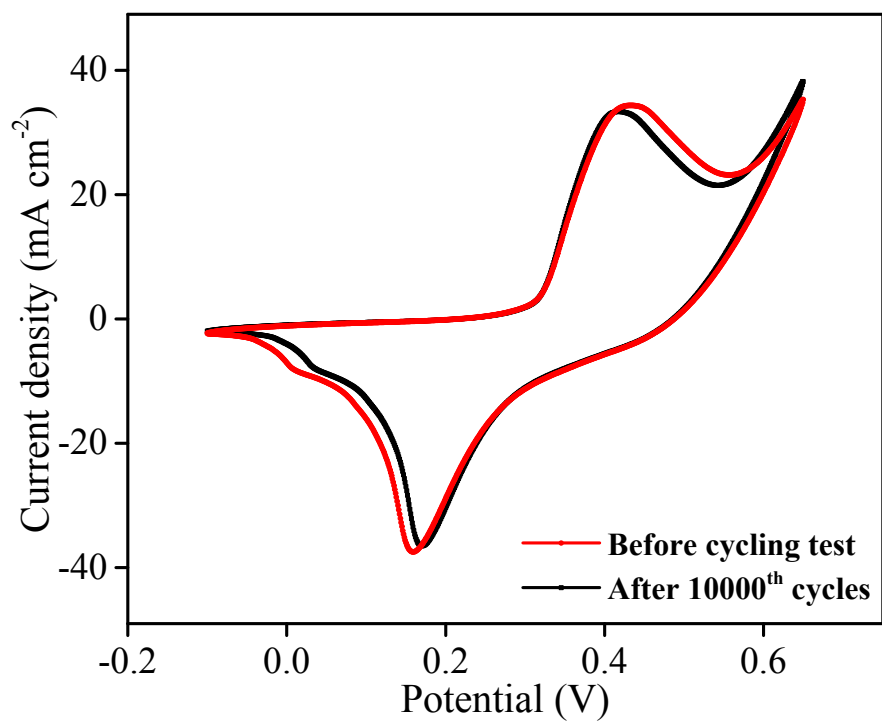


Fig. S11. CV curves of $\text{Cu}_{1-x}\text{Ni}_x\text{S}$ electrode at 10 mV s^{-1} (before and after 10000 cycling performance).

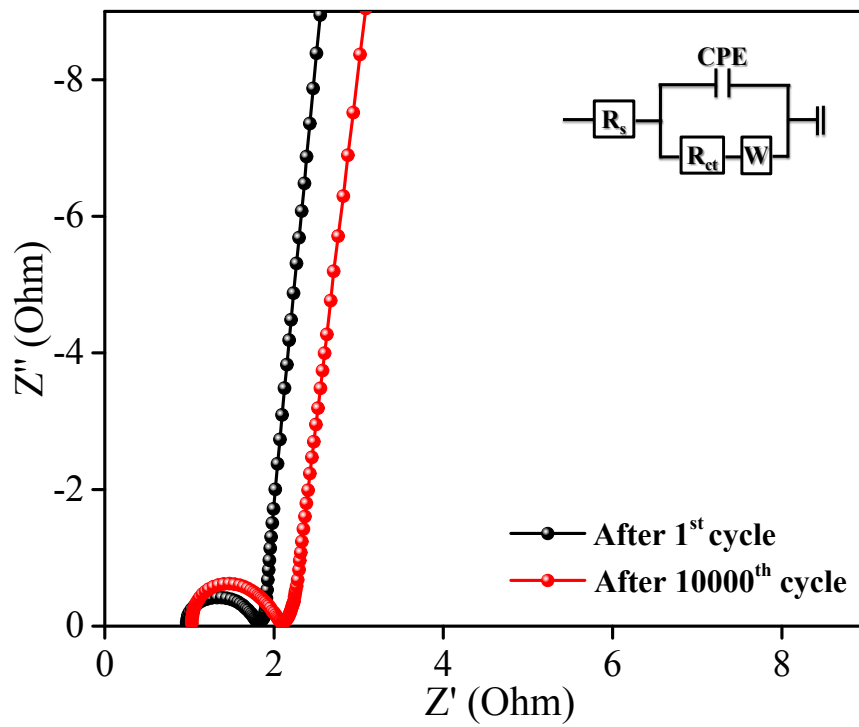


Fig. S12. EIS of $\text{Cu}_{1-x}\text{Ni}_x\text{S}$ electrode during the cycling performance test.

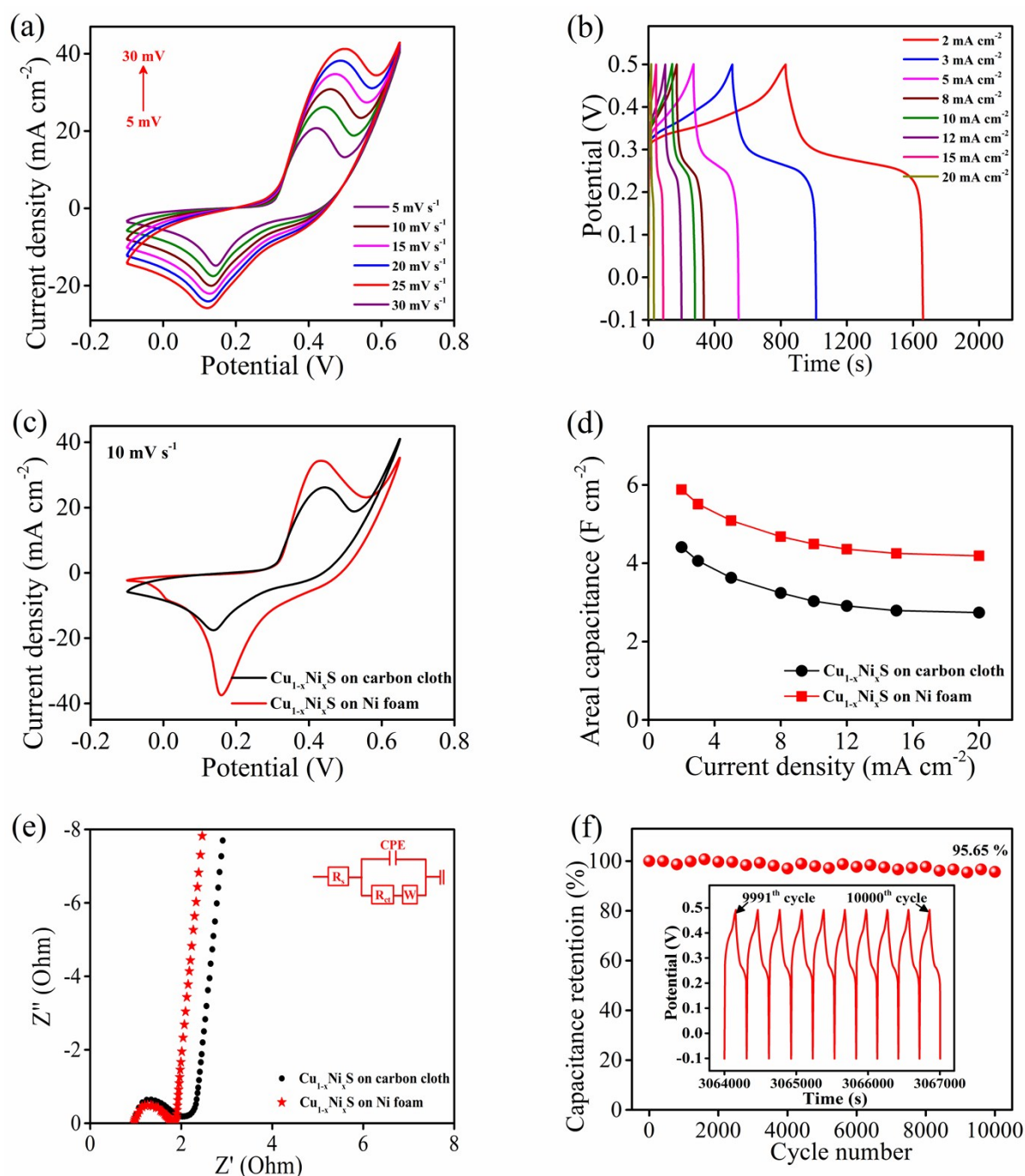


Fig. S13. Electrochemical characterization of the carbon cloth supported $\text{Cu}_{1-x}\text{Ni}_x\text{S}$ nanosheet arrays electrode: (a) CVs at different scan rates, (b) GCDs at different current densities of carbon cloth supported $\text{Cu}_{1-x}\text{Ni}_x\text{S}$ nanosheet arrays electrode, (c) CV curves of carbon cloth and Ni foam supported $\text{Cu}_{1-x}\text{Ni}_x\text{S}$ nanosheet arrays at a scan rate of 10 mV s^{-1} , (d) Areal capacitance of carbon cloth and Ni foam supported $\text{Cu}_{1-x}\text{Ni}_x\text{S}$ nanosheet arrays at different current densities. (e) EIS of carbon cloth and Ni foam supported $\text{Cu}_{1-x}\text{Ni}_x\text{S}$ nanosheet arrays, and (f) Cycling performance of carbon cloth supported $\text{Cu}_{1-x}\text{Ni}_x\text{S}$ nanosheet arrays electrode at

a current density of 12 mA cm^{-2} (inset: GCD curves of carbon cloth supported $\text{Cu}_{1-x}\text{Ni}_x\text{S}$ nanosheet arrays electrode curves from 9991th to 10,000th cycles).

The CV curves at different scan rate of the carbon cloth supported $\text{Cu}_{1-x}\text{Ni}_x\text{S}$ nanosheet arrays with a potential window from -0.1 to 0.65 V , as shown in Fig. 13a. All of the CV curves consist of a pair of strong redox peak, specifically at low scan rates, showing exceptional redox behaviour of $\text{Cu}_{1-x}\text{Ni}_x\text{S}$ during the electrochemical performance. When the scan rate increases from 5 to 30 mV s^{-1} , the CVs area also increases and the shapes are well maintained at a high scan rate, which reveals that the superior electrocatalytic activity of $\text{Cu}_{1-x}\text{Ni}_x\text{S}$ nanosheet arrays. The GCD curves of carbon cloth supported $\text{Cu}_{1-x}\text{Ni}_x\text{S}$ nanosheet arrays with different current densities from 2 to 20 mA cm^{-2} are shown in Fig. S13b. The GCD curves confirm that highly reversible charge/discharge behaviour of $\text{Cu}_{1-x}\text{Ni}_x\text{S}$ nanosheet arrays. All GCD curves exhibit the carbon cloth supported $\text{Cu}_{1-x}\text{Ni}_x\text{S}$ nanosheet arrays electrode characteristics with pseudocapacitive behaviour, which is well-consistent with CV study. The areal capacitance (C_A) of the carbon cloth supported $\text{Cu}_{1-x}\text{Ni}_x\text{S}$ nanosheet arrays from the discharge curves of the GCD were calculated and are found to be $\sim 4.41, 4.06, 3.63, 3.24, 3.03, 2.91, 2.79$ and 2.74 F cm^{-2} at the current densities of $2, 3, 5, 8, 10, 12, 15,$ and 20 mA cm^{-2} respectively. The carbon cloth supported $\text{Cu}_{1-x}\text{Ni}_x\text{S}$ nanosheet arrays shows better electrochemical performance because of their high specific surface area with unique porous architectures. But the areal capacitance of the carbon cloth supported $\text{Cu}_{1-x}\text{Ni}_x\text{S}$ nanosheet arrays ($C_A = 4.41 \text{ F cm}^{-2}$) is still lower than that of Ni foam supported $\text{Cu}_{1-x}\text{Ni}_x\text{S}$ nanosheet arrays ($C_A = 5.88 \text{ F cm}^{-2}$), which is due to the substrate effect. Therefore, we conclude that the the substrate, Ni foam also contributes to the capacitive performance.

The standardized CV curves of the two kinds of $\text{Cu}_{1-x}\text{Ni}_x\text{S}$ nanosheet arrays grown over different substrates (current collector) at 10 mV s^{-1} give a survey of the capacitive properties (Fig. 13c). The Ni foam supported $\text{Cu}_{1-x}\text{Ni}_x\text{S}$ nanosheet arrays exhibit larger CV areas than that of carbon cloth supported $\text{Cu}_{1-x}\text{Ni}_x\text{S}$ nanosheet arrays, which reveals that the larger areal/specific capacitance. Besides, the Ni foam supported $\text{Cu}_{1-x}\text{Ni}_x\text{S}$ nanosheet arrays possess areal capacitance values of $\sim 5.88, 5.51, 5.09, 4.68, 4.49, 4.36, 4.25,$ and 4.19 F cm^{-2} at the current densities of 2, 3, 5, 8, 10, 12, 15, and 20 mA cm^{-2} respectively (Fig. S13d). This study reveals that the Ni foam supported $\text{Cu}_{1-x}\text{Ni}_x\text{S}$ nanosheet arrays showed the areal capacitance of 5.88 F cm^{-2} and specific capacitance of 2672 F g^{-1} at a current density of 2 mA cm^{-2} which is higher than that of the carbon cloth supported $\text{Cu}_{1-x}\text{Ni}_x\text{S}$ nanosheet arrays ($C_A = 4.41 \text{ F cm}^{-2}$; $C_s = 2384 \text{ F g}^{-1}$). Further, the charge transfer resistances (R_{ct}) of the Ni foam and carbon cloth supported $\text{Cu}_{1-x}\text{Ni}_x\text{S}$ nanosheet arrays electrodes were examined by EIS technique, as illustrated in Fig. S13e. The Ni foam supported $\text{Cu}_{1-x}\text{Ni}_x\text{S}$ nanosheet arrays electrode demonstrates low resistances ($R_s = 0.96 \Omega$, $R_{ct} = 1.28 \Omega$) when compared to that of carbon cloth supported $\text{Cu}_{1-x}\text{Ni}_x\text{S}$ nanosheet arrays ($R_s = 0.98 \Omega$, $R_{ct} = 1.41 \Omega$). It clearly reveals that the Ni foam supported $\text{Cu}_{1-x}\text{Ni}_x\text{S}$ nanosheet arrays shows a better electron/ion transport kinetics than that of carbon cloth supported $\text{Cu}_{1-x}\text{Ni}_x\text{S}$ nanosheet arrays electrode.¹

The cycling stability of the carbon cloth supported $\text{Cu}_{1-x}\text{Ni}_x\text{S}$ nanosheet arrays electrodes were examined at a GCD current density of 12 mA cm^{-2} in the potential range of -0.1 to 0.5 V for 10,000 continuous cycles, as shown in Fig. S13f. In case of the carbon cloth supported $\text{Cu}_{1-x}\text{Ni}_x\text{S}$ electrode, $\sim 95.65\%$ of the initial areal capacitance was retained after 10,000 repetitive cycling tests. The GCD curves of the carbon cloth supported $\text{Cu}_{1-x}\text{Ni}_x\text{S}$ from the 9,991th to the 10,000th cycles are shown in inset Fig. S13f. The last 10 GCD curves display minor changes when compared to the first 10 GCD curves, which reveals that the carbon cloth supported $\text{Cu}_{1-x}\text{Ni}_x\text{S}$

$_{x}\text{Ni}_x\text{S}$ electrode also holds good cycling stability. This cycling performance is mainly attributed to enhanced electrical conductivity of the electrode materials, which is in good agreement with EIS study. The Ni foam and carbon cloth supported $\text{Cu}_{1-x}\text{Ni}_x\text{S}$ nanosheet arrays showed ~97.33% and ~95.65% of the capacitance retentions of the initial capacitance after 10,000 repetitive cycling tests, which confirms that exceptional cycling stability at higher current density of 12 mA cm^{-2} . The stabilities of these above two different current collector supported electrodes may result from the different densities of the $\text{Cu}_{1-x}\text{Ni}_x\text{S}$ nanosheet arrays on the conductive substrates. The higher density of $\text{Cu}_{1-x}\text{Ni}_x\text{S}$ nanosheet arrays on the carbon cloth current collector, the electrode is adverse for the penetration of the electrolyte.¹⁻² From the above discussion, we conclude that the Ni foam is one of the best support for designing $\text{Cu}_{1-x}\text{Ni}_x\text{S}$ nanosheet arrays. Therefore, we further process the electrochemical performance study using Ni foam supported $\text{Cu}_{1-x}\text{Ni}_x\text{S}$ nanosheet arrays.

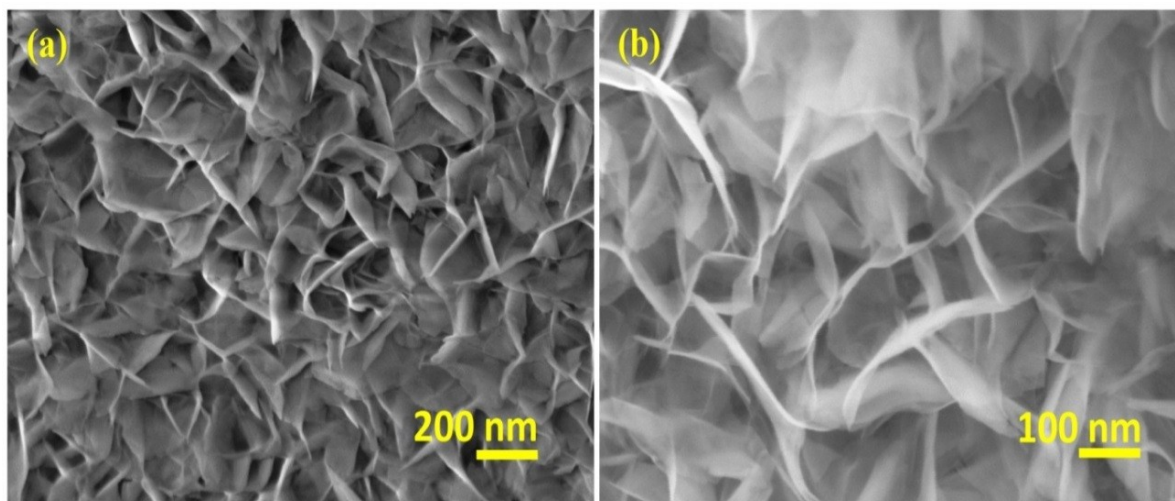


Fig. S14. SEM images with different magnifications of $\text{Cu}_{1-x}\text{Ni}_x\text{S}$ nanosheet arrays supported on porous 3D Ni backbone (after 10000 cycling performance).

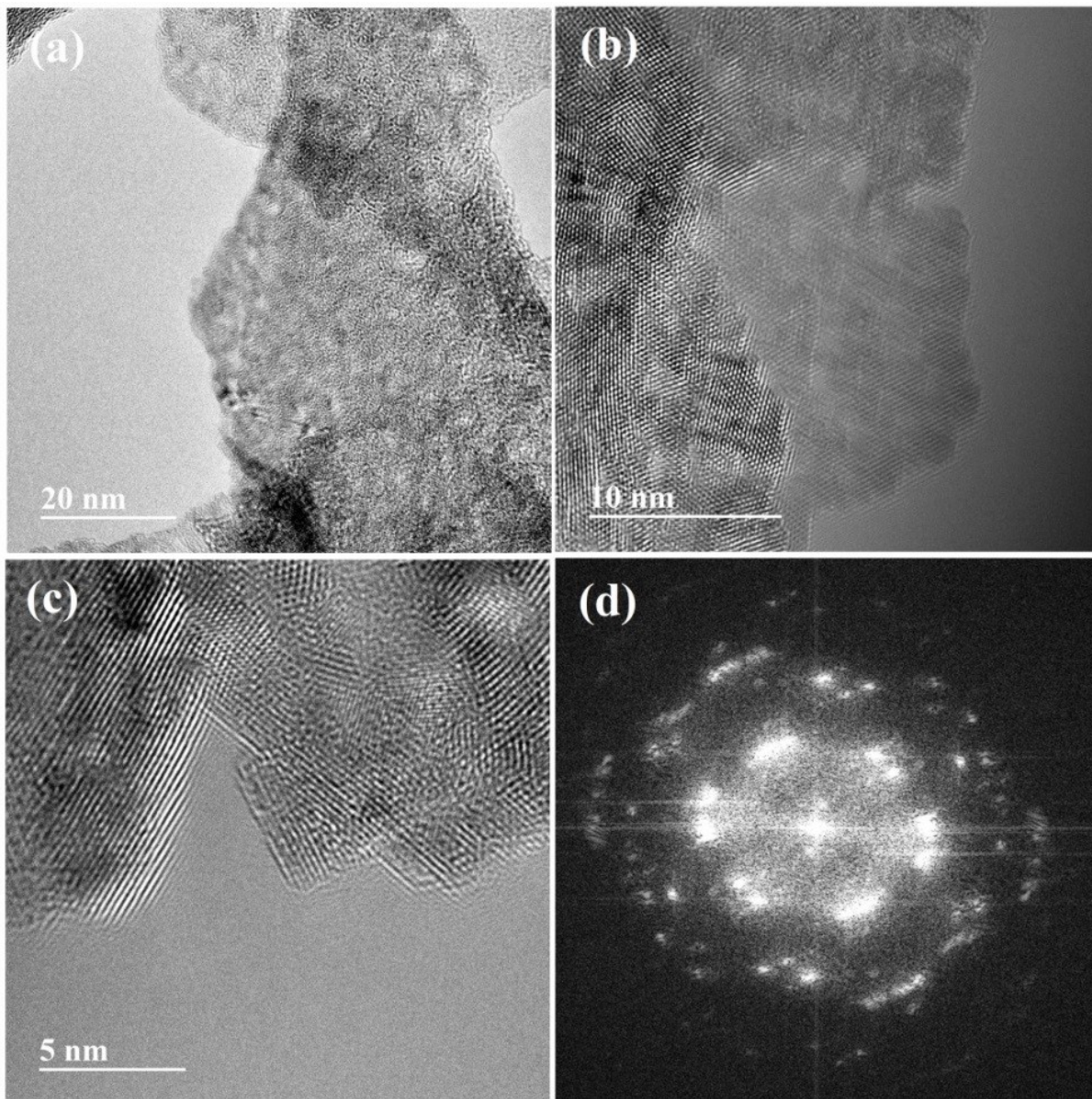


Fig. S15. (a–c) TEM images with different magnifications, (d) FFT of $\text{Cu}_{1-x}\text{Ni}_x\text{S}$ nanosheet arrays (after 10,000 cycling test).

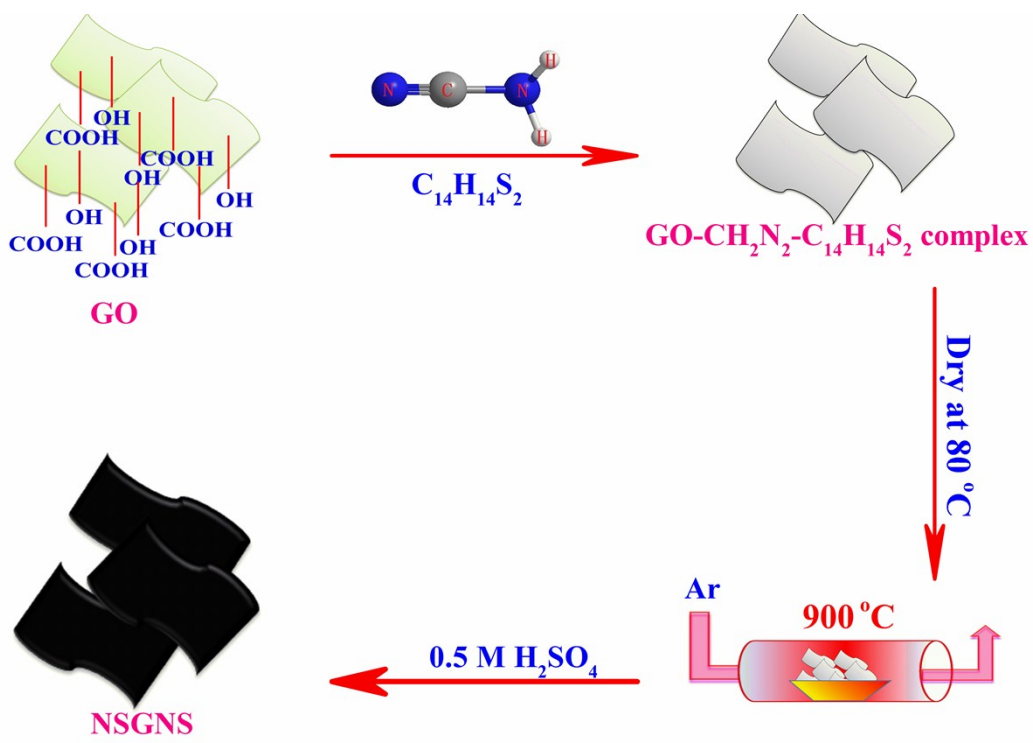


Fig. S16. Schematic illustration for the synthesis of NSGNS by in-situ two step methods.

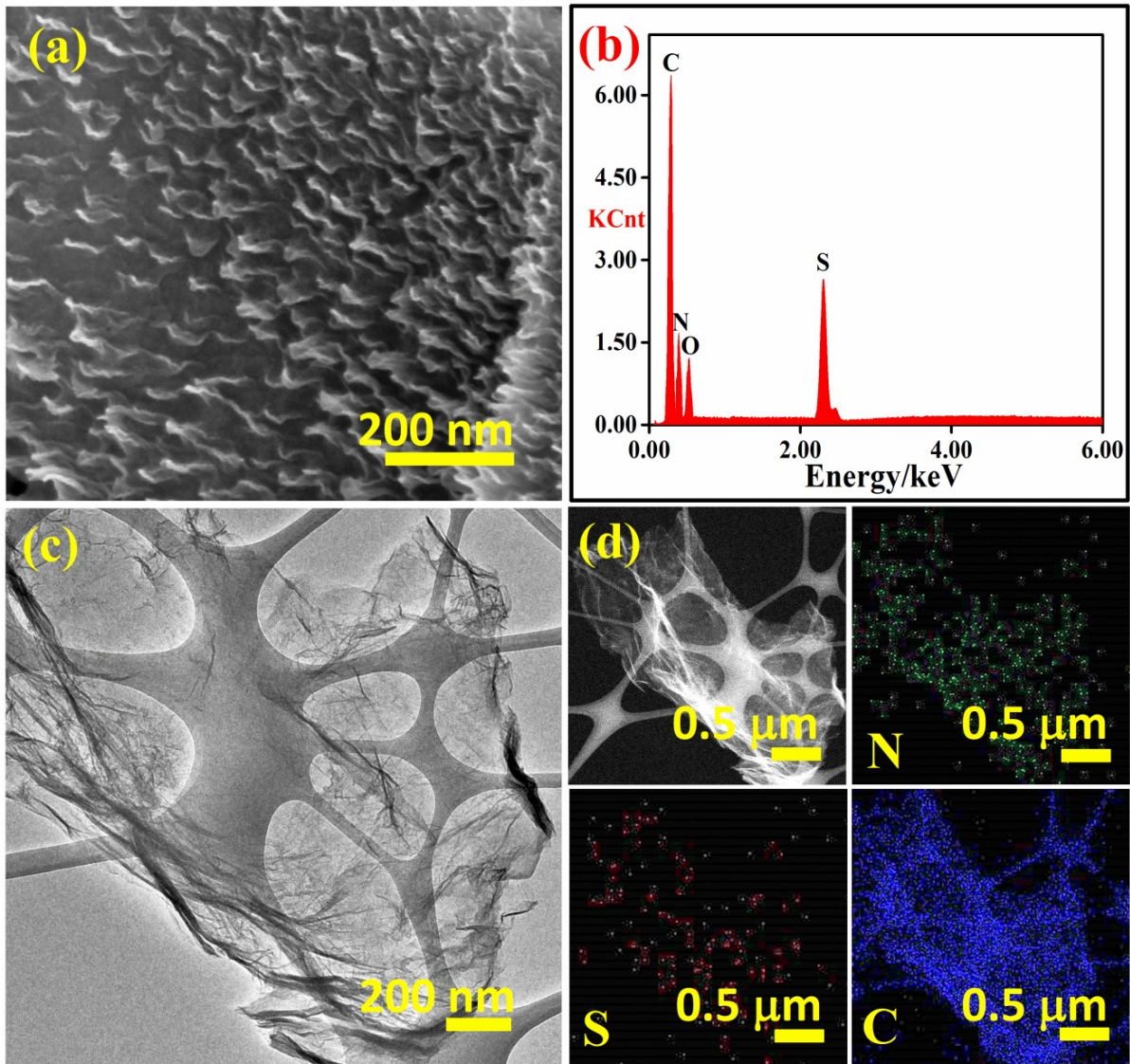


Fig. S17. (a) FE-SEM image, (b) EDAX spectra, (c) TEM image of as-synthesized NSGNS, (d) SETM image of as-synthesized NSGNS and its corresponding STEM/EDS color elemental mappings of N-K, S-K and C-K.

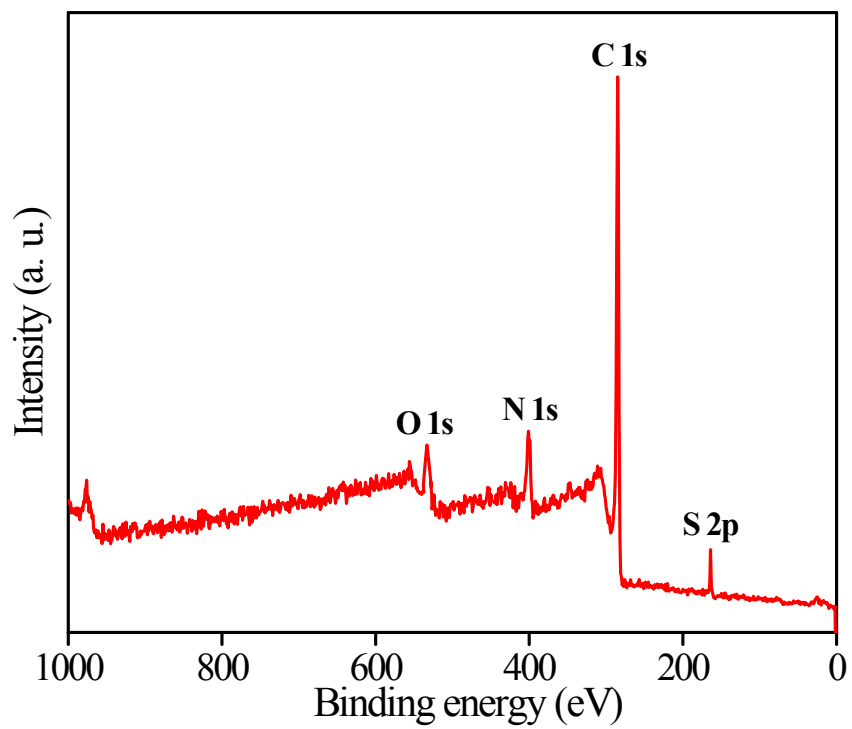


Fig. S18. (a) XPS survey spectrum of NSGNS.

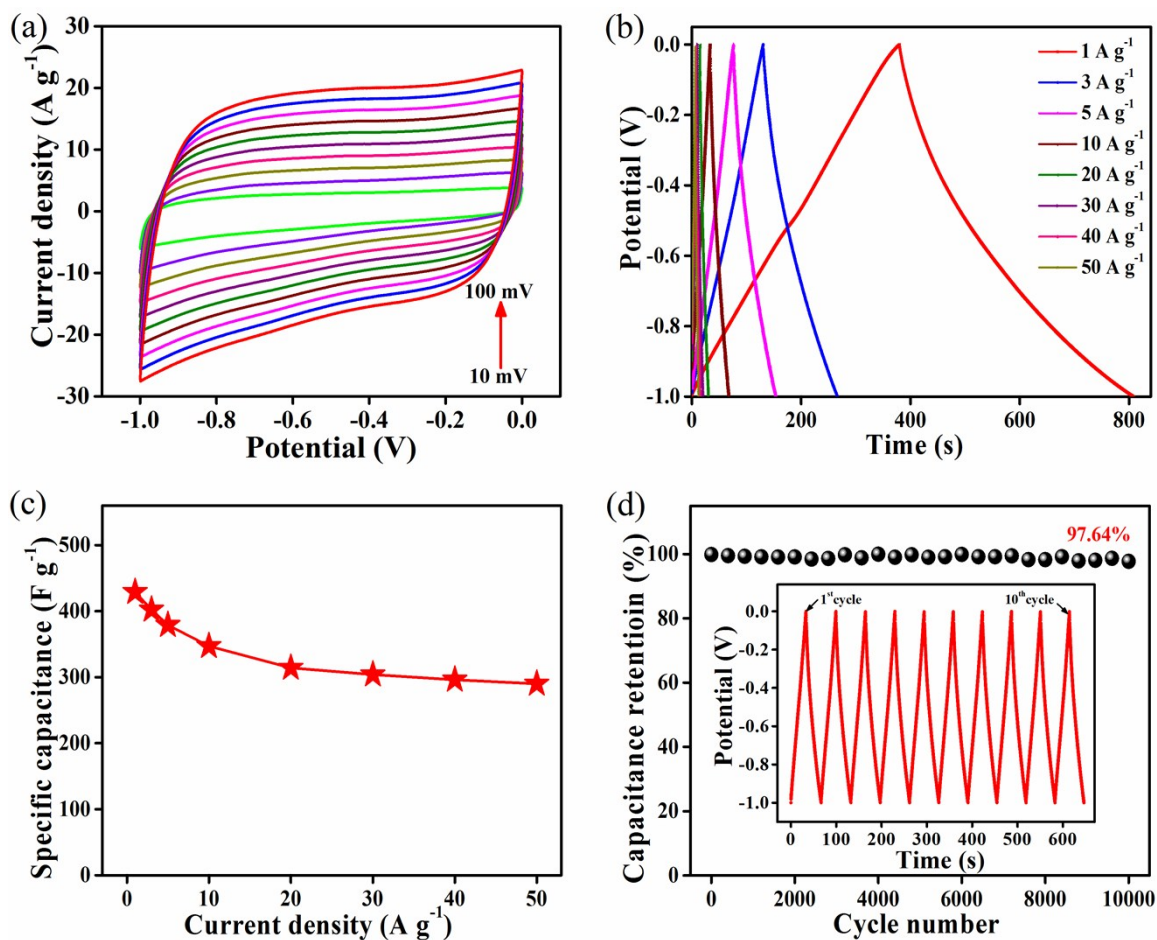


Fig. S19. (a) CV curves of NSGNS at different sweep rates from 10 to 200 mV s⁻¹, and (b) GCD curves of NSGNS at the current densities of 1, 3, 5, 10, 20, 30, 40 and 50 A g⁻¹, (c) specific capacitances vs current densities, and (d) Cycling performance of NSGNS electrode at the current density of 10 A g⁻¹, inset showing GCD curves of NSGNS curves from 1st to 10th cycles.

To investigate the electrochemical performance of the NSGNS electrode, tests are carried out in a three-electrode system with 2 M KOH electrolyte (Fig. S19). The CV curves with different sweep rates (10 to 100 mV s⁻¹) of NSGNS electrode are illustrated in Fig. S19a. All CV curves well maintained the rectangular shape without any distortion, which confirms that the ideal capacitive behaviour and fast ion/electron transport transport takes place in the NSGNS. The NSGNS electrode showed excellent symmetric charge-discharge performance with high specific capacitance. The GCD curves are with different current densities (1 to 50 A

g^{-1}) of NSGNS to the prolonged potential window of -1.0 to 0 V are not shown in Fig. S19b. The specific capacitance of the NSGNS electrode from the discharge curves of the GCD were calculated to be $\sim 425, 402, 379, 347, 314, 305, 296,$ and 290 F g^{-1} at the current densities of $1, 3, 5, 10, 20, 30, 40$ and 50 A g^{-1} , respectively. The NSGNS achieved ultra-high specific capacitance of $\sim 425 \text{ F g}^{-1}$ at a current density of 1 A g^{-1} . At a current density of 50 A g^{-1} , the specific capacitance of the NGNS is $\sim 290 \text{ F g}^{-1}$, which further confirms the exceptional rate capability. The specific capacitance vs current density of the NGNS consequences based on the discharge curves are shown in Fig. S19c. The long-term cycling stability of the NSGNS exhibits negligible deterioration of the initial capacitance after $10,000$ consecutive GCD tests at a current density of 10 A g^{-1} (Fig. S19d). The consecutive GCD curves of the NSGNS 10 cycles test are illustrated in the inset of Fig. S19d, demonstrating in negligible changes are attained. This result further confirms that NSGNS electrode is superior and ultra-high electrode for supercapacitors. Therefore, NSGNS material possesses ultra-high specific capacitance, excellent rate capability, and outstanding cycling life when compared to recently reported heteroatom doped graphene-based electrode materials, which is credited to the unique porous architecture and ultra-high surface area of NSGNS.³ The superior electrochemical performance of the NSGNS makes it the best material for the negative electrode in this current research work.

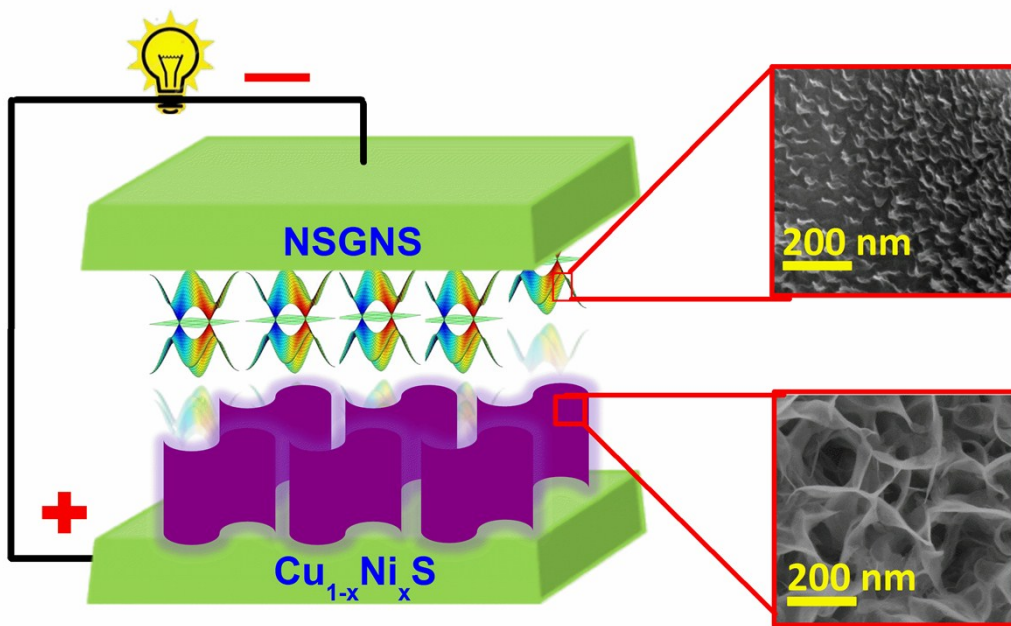


Fig. S20. Schematic illustration of the asymmetric all-solid-state supercapacitors.

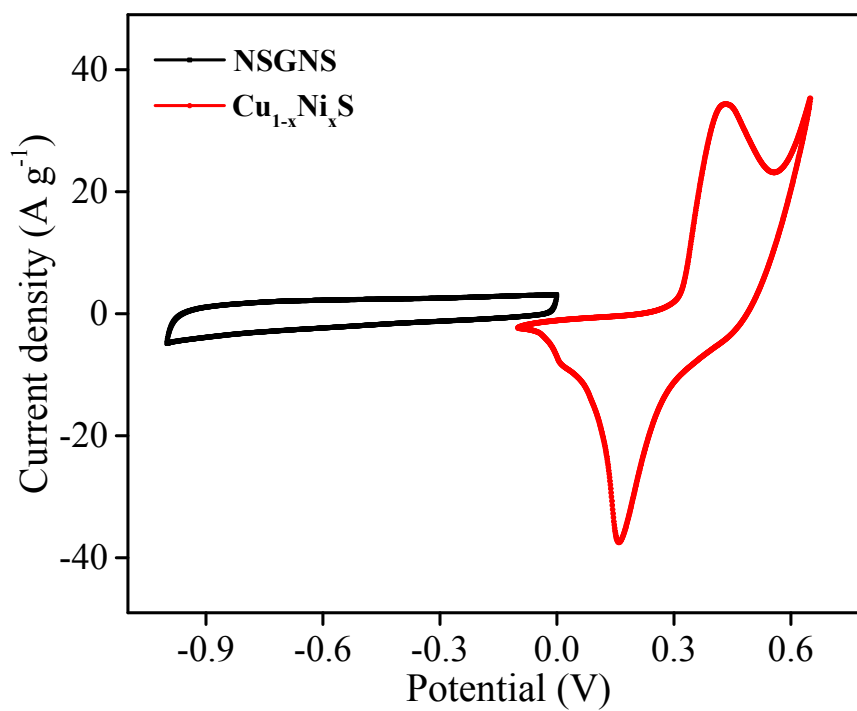


Fig. S21. Cu_{1-x}Ni_xS and NSGNS electrodes measured at a scan rate of 10 mV s⁻¹ in a three electrode system.

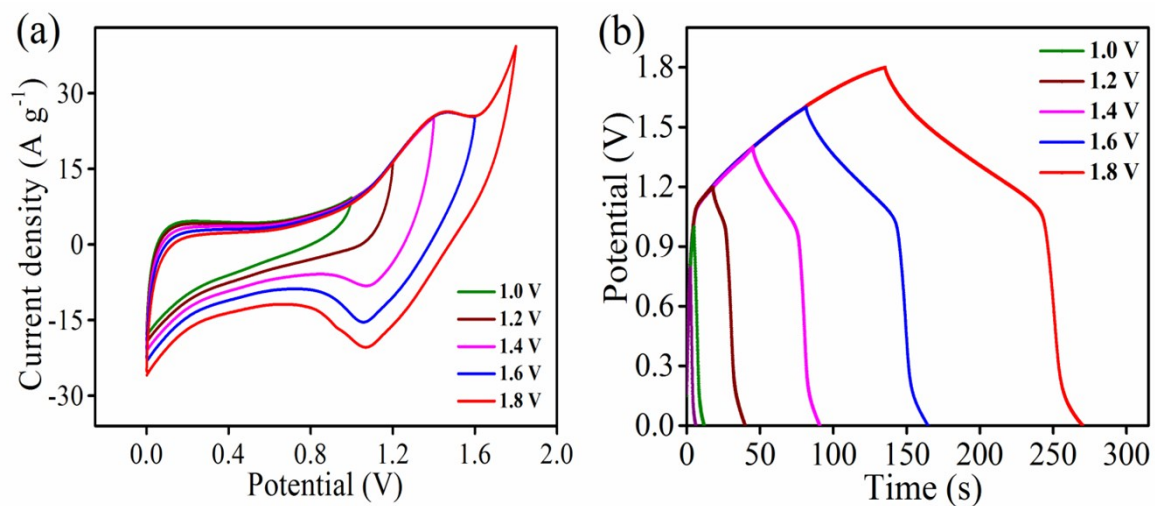


Fig. S22. CV curves (scan rate 50 mV s^{-1}) of the optimized $\text{Cu}_{1-x}\text{Ni}_x\text{S//NSGNS}$ ASC device measured at different voltage windows from 1.0 to 1.8 V, (b) GCD curves (at a current density of 2 A g^{-1}) of $\text{Cu}_{1-x}\text{Ni}_x\text{S//NSGNS}$ ASCs device collected at different potential windows from 1.0 to 1.8 V.

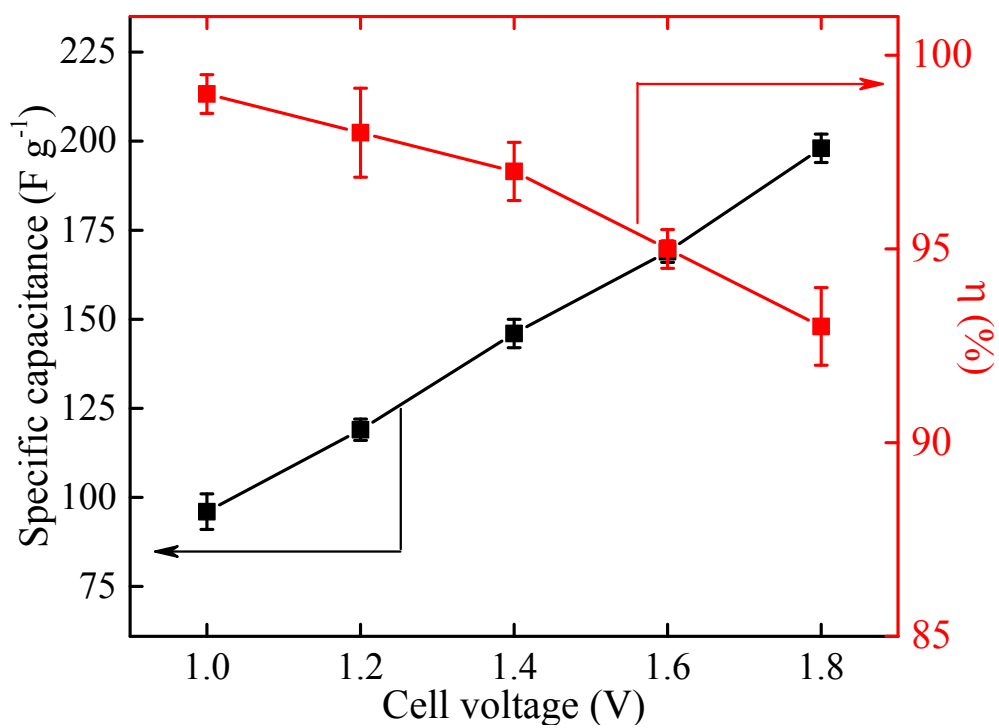


Fig. S23. Coulombic efficiency and specific capacitance of a ASC in solid-state KOH-PVA electrolyte vs different cell voltage.

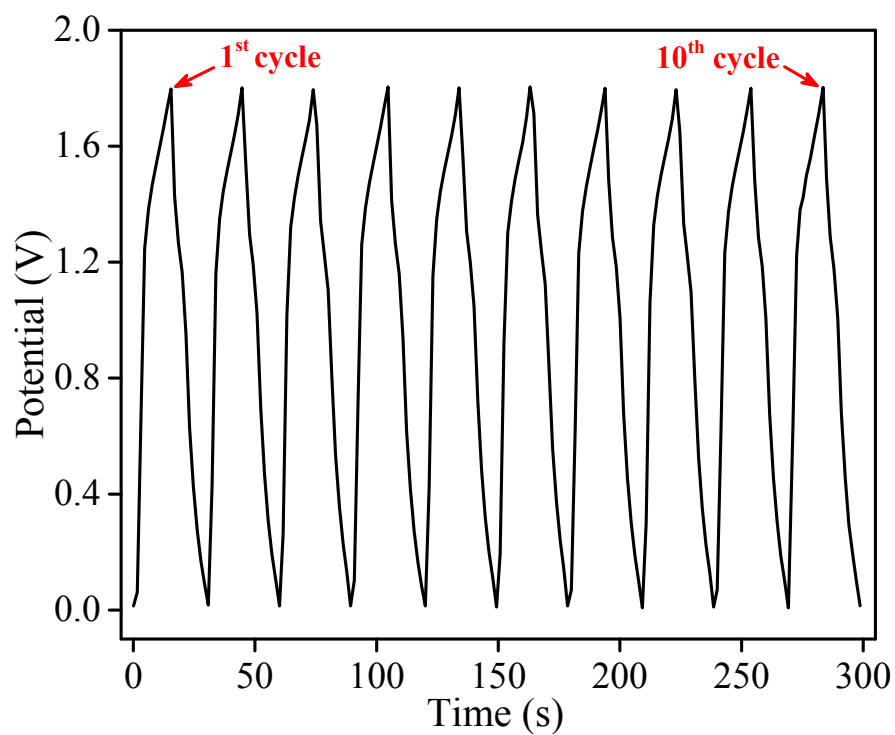


Fig. S24. GCD curves of $\text{Cu}_{1-x}\text{Ni}_x\text{S}/\text{NSGNS}$ ASCs device: from the 1st to 10th cycles test.

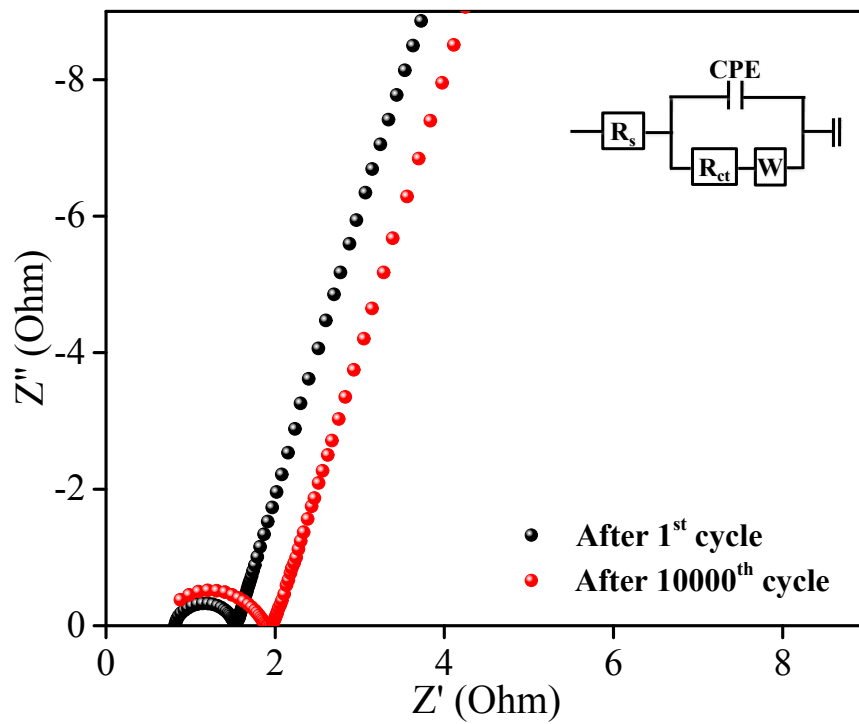


Fig. S25. EIS of $\text{Cu}_{1-x}\text{Ni}_x\text{S}$ //NSGNS ASC device during the cycling performance test.

Table S1. Chemical composition of $\text{Cu}_{1-x}\text{Ni}_x$ DHs, $\text{Cu}_{1-x}\text{Ni}_x\text{O}$, and $\text{Cu}_{1-x}\text{Ni}_x\text{S}$ nanosheet arrays estimated from XPS and ICP-AES

Sample	Cu (at. %)	Ni (at. %)	S (at. %)	O (at. %)
$\text{Cu}_{1-x}\text{Ni}_x$ DHs	30.56	32.18	-	25.76
$\text{Cu}_{1-x}\text{Ni}_x\text{O}$	30.14	30.98	-	30.98
$\text{Cu}_{1-x}\text{Ni}_x\text{S}$	29.04	31.09	20.78	11.09

Cu, Ni, S and O contents were detected by XPS analysis and ICP-AES measurements

Table S2. Electrode properties comparison with reported literatures

Materials	Specific capacitance (F g ⁻¹)	Areal capacitance (F cm ⁻²)	Current load or scan rate	Electrolyte	Stability	References
NiCo ₂ S ₄ hollow spheres	1036		1 A g ⁻¹	6 M KOH	87% (2000cycles)	4
NiCo ₂ S ₄ /CNF	-	2.86	4 mA cm ⁻²	1 M KOH	96% (2000cycles)	5
Ni-Co-S	1418	-	5 A g ⁻¹	1 M KOH	-	6
Ni _x Co _{3-x} S ₄ hollow	895.2	-	1 A g ⁻¹	2 M KOH	86.5% (1500 cycles)	7
NiCo ₂ S ₄ hollow nanoneedle	1154	-	1 A g ⁻¹	2 M KOH	98.2% (8000cycles)	8
FeCo ₂ S ₄ -NiCo ₂ S ₄ Composite	1518.5	3.5	5 mA cm ⁻²	3 M KOH	77% (3000cycles)	9
Co ₉ S ₈ /NF	1646	-	3 A g ⁻¹	2 M KOH	94.4% (2000cycles)	10
NiCo ₂ S ₄ /NC F	1231	-	2 A g ⁻¹	6 M KOH	90.4% (2000cycles)	11
MoS ₂ /PPy	700	-	0.5 A g ⁻¹	1 M KCl	85% (4000 cycles)	12
porous Co-Al hydroxide nanosheets	1043	-	1 A g ⁻¹	6 M KOH	88% (3000 cycles)	13
CoS ₂ hollow sphere	1301	-	1 A g ⁻¹	2 M KOH	90.1% (2000 cycles)	14
Cu ₇ S ₄ nanowire	400	-	10 mV s ⁻¹	LiCl-PVA gel	95% (5000 cycles)	15
NiCo-carbonate hydroxide	1398	-	1 A g ⁻¹	6 M KOH	95% (2500 cycles)	16
KCu ₇ S ₄ /GP	483	1.75	0.4 mA cm ⁻²	H ₃ PO ₄ -PVA	60% (200 cycles)	17
FeCo ₂ S ₄	2411	-	2 mA cm ⁻²	3 M KOH	72% (5000 cycles)	18
Ni-Co-S/G//PCNS	1492	-	1 A g ⁻¹	6 M KOH	90% (8000 cycles)	19

Cu _{1-x} Ni _x S nanosheet	2673	5.88	2 mA cm ⁻²	2 M KOH	97.33% (10,000 cycles)	This work
--	------	------	--------------------------	---------	---------------------------	--------------

NCF: nitrogen-doped carbon foams; NF: nickel foam

Table S3. ASC Device properties comparison with recently reported literatures

Reported ASC Device	Electrolyte	Device Window (V)	Energy Density (Wh kg ⁻¹)	Power Density (W kg ⁻¹)	Stability (Cycle No.)	Reference
FeCo ₂ S ₄ //3D PNG	KOH/PVA	0-1.6	76.1	755	82% (10000 cycles)	18
NiCo ₂ S ₄ //G/CS	6 M KOH	0-1.6	42.3	476	78.6% (10000 cycles)	4
NiCo ₂ S ₄ //CFP-AC	2 M KOH	0-1.5	86.6	200	88.6% (5000 cycles)	8
Ni-Co-S/G//PCNS	6 M KOH	0-1.6	43.3	800	85% (10000 cycles)	19
NiCo ₂ S ₄ /NCF//OMC/NCF	6 M KOH	0-1.6	45.5	512	70.4% (10000 cycles)	11
CuCo ₂ S ₄ -HNN//AC	3 M KOH	0-1.6	44.1	800	94.1% (6000 cycles)	20
NiCo ₂ S ₄ //rGO	PVA/KOH	0-1.5	38.64	1330	99.3% (5000 cycles)	21
NiCo ₂ S ₄ @NiO NWAs//AC	3 M KOH	0-1.6	30.38	288	109% (5000 cycles)	22
Ni-Co-S//graphene	1 M KOH	0-1.75	60	1800	90.1% (10000 cycles)	6
Ni-Co LDH//RGO	1 M KOH	0-1.6	77.3	623	82% (5000 cycles)	23
NiCo ₂ S ₄ nanotube array//carbon aerogel	2 M KOH	0-1.6	55.3	400	96.6% (5000 cycles)	24
Ni-Co-S//AC	6 M KOH	0-1.8	41.4	414	93.5% (6000 cycles)	25
Co ₃ O ₄ //carbon	6 M KOH	0-1.6	36	800	89% (2000 cycles)	26

Cu _{1-x} Ni _x S//NSGNS	PVA-KOH	0-1.8	94.05	1085	95.86% (10000 cycles)	This work
--	---------	-------	-------	------	-----------------------------	--------------

NCF: nitrogen-doped carbon foams; NF: nickel foam

Notes and references

1. Y. Ma, Y. Jia, L. Wang, M. Yang, Y. Bi and Y. Qi, *RSC Adv.*, 2016, **6**, 12093-12099.
2. F. X. Bao, Z. Q. Zhang, W. Guo and X. Liu, *Electrochim Acta*, 2015, **157**, 31–40.
3. P. Chen, J. J. Yang, S. S. Li, Z. Wang, T. Y. Xiao, Y. H. Qian and S. H. Yu, *Nano Energy*, 2013, **2**, 249-256.
4. L. Shen, L. Yu, H. B. Wu, X. Y. Yu, X. Zhang and X. W. Lou, *Nat. Commun.*, 2015, **6**, 6694.
5. J. Xiao, L. Wan, S. Yang, F. Xiao and S. Wang, *Nano Lett.*, 2014, **14**, 831-838.
6. W. Chen, Ch. Xia and H. N. Alshareef, *ACS Nano*, 2014, **8**, 9531-9541.
7. L. Yu, L. Zhang, H. B. Wu and X. W. Lou, *Angew. Chem.*, 2014, **126**, 3785-3788.
8. X. Xiong, G. Waller, D. Ding, D. Chen, B. Rainwater, B. Zhao, Z. Wang, M. Liu, *Nano Energy*, 2015, **16**, 71-80.
9. J. Zhu, S. Tang, J. Wu, X. Shi, B. Zhu and X. Meng, *Adv. Energy Mater.*, 2017, **7**, 1601234.
10. V. Viswanathan, K. L. Pickrahn, A. C. Luntz, S. F. Bent and J. K. Nørskov, *Nano Lett.*, 2015, **15**, 6689-6695.
11. L. Shen, J. Wang, G. Xu, H. Li, H. Dou and X. Zhang, *Adv. Energy Mater.*, 2015, **5**, 1400977.
12. H. Tang, J. Wang, H. Yin, H. Zhao, D. Wang and Z. Tang, *Adv. Mater.*, 2015, **27**, 1117-1123.
13. X. Wu, L. Jiang, C. Long, T. Wei and Z. Fan, *Adv. Funct. Mater.*, 2015, **25**, 1648-1655.
14. S. Peng, L. Li, H. Tan, R. Cai, W. Shi, C. Li, S. G. Mhaisalkar, M. Srinivasan, S. Ramakrishna and Q. Yan, *Adv. Funct. Mater.*, 2014, **24**, 2155-2162.

15. M. S. Javed, S. Dai, M. Wang, Y. Xi, Q. Lang, D. Guo and C. Hu, *Nanoscale*, 2015, **7**, 13610-13618.
16. J. Yang, C. Yu, X. Fan, C. Zhao and J. Qiu, *Adv. Funct. Mater.*, 2015, **25**, 2109-2116.
17. S. Dai, W. Xu, Y. Xin, M. Wang, X. Gun, D. Guo and C. Hu, *Nano Energy*, 2016, **19**, 363-372.
18. S. Tang, B. Zhu, X. Shi, J. Wu and X. Meng, *Adv. Energy Mater.*, 2017, 1601985.
19. J. Yang, C. Yu, X. Fan, S. Liang, S. Li, H. Huang, Z. Ling, C. Hao and J. Qiu, *Energy Environ. Sci.*, 2016, **9**, 1299-1307.
20. S. E. Moosavifard, S. Fani and M. Rahmanian, *Chem. Commun.*, 2016, **52**, 4517-4520.
21. F. Lu, M. Zhou, W. Li, Q. Weng, C. Li, Y. Xue, X. Jiang, X. Zeng, Y. Bando and D. Golberg, *Nano Energy*, 2016, **26**, 313-323.
22. Y. Huang, T. Shi, S. Jiang, S. Cheng, X. Tao, Y. Zhong, G. Liao and Z. Tang, *Sci. Report*, 2016, **6**, 38620.
23. H. Chen, L. Hu, M. Chen, Y. Yan and L. Wu, *Adv. Funct. Mater.*, 2014, **24**, 934-942.
24. P. Hao, J. Tian, Y. Sang, C. C. Tuan, G. Cui, X. Shi, C.P. Wong, B. Tang and H. Liu, *Nanoscale*, 2016, **8**, 16292-16301.
25. X. Li, Q. Li, Y. Wu, M. Rui and H. Zeng, *ACS Appl. Mater. Interfaces*, 2015, **7**, 19316-19323.
26. R. R. Salunkhe, J. Tang, Y. Kamachi, T. Nakato, J. H. Kim and Y. Yamauchi, *ACS Nano*, 2015, **9**, 6288-6296.